Developmental Cell, Volume *26*

Supplemental Information

Advances in Analysis of Low Signal-to-Noise Images Link Dynamin and AP2 to the Functions of an Endocytic Checkpoint

François Aguet, Costin N. Antonescu, Marcel Mettlen, Sandra L. Schmid, and Gaudenz Danuser

Inventory of supplemental materials:

- **Supplemental Figures S1–S4**
  Figure S1, related to Figure 1
  Figure S2, related to Figure 1
  Figure S3, related to Figure 3
  Figure S4, related to Figure 5
- **Supplemental Movies S1–S4**
  Movie S1, related to Figure 1
  Movie S2, related to Figure 1
  Movie S3, related to Figure 4
  Movie S4, related to Figure 5
- **Supplemental Experimental Procedures**
- **Supplemental References**
- **Supplemental Software**

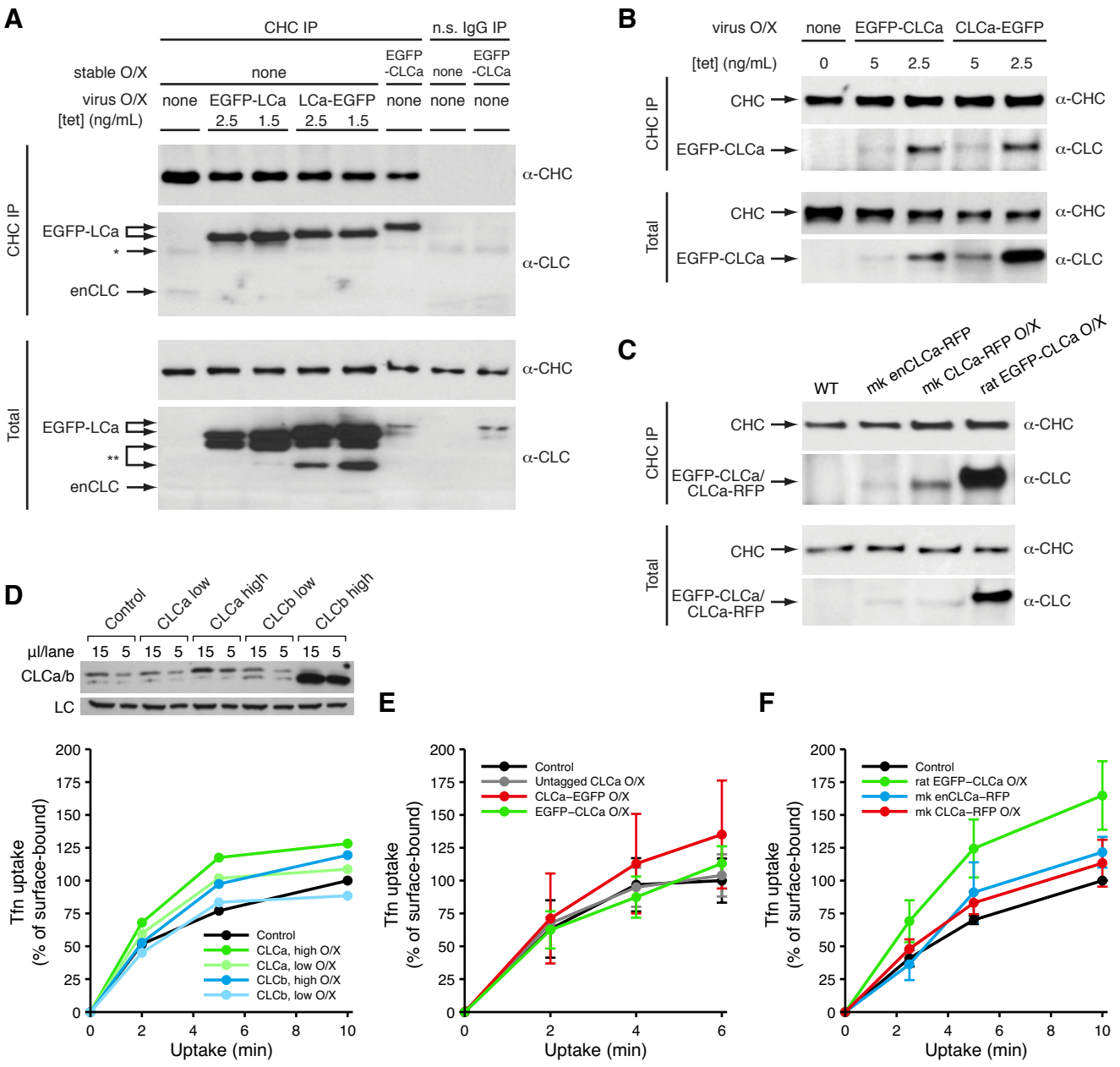

Figure S1. Over-expressed clathrin light chains are incorporated into clathrin triskelions and do not affect CME, related to Figure 1 (A) Clathrin heavy chain (CHC) was immunoprecipitated from cells overexpressing either N- or C-terminally EGFP-tagged rat CLCa from tet-regulatable adenoviral vectors. The fluorescently-tagged light chains are incorporated into clathrin triskelions at a much higher stoichiometry than endogenous CLCa in uninfected control cells or in genome-edited enEGFP-CLCa cells. Unincorporated CLCa is partially degraded as can be seen in western blots of the whole cell lysate (total). * indicates a non-specific band and ** indicates degradation products. **(B)** N-terminally tagged CLCa is more efficiently incorporated into triskelions than C-terminaly-tagged CLCa, although both are co-precipitated with CHC. **(C)** CLCa from monkey and rat are equally efficiently incorporated into CHC in monkey BSC1 cells. **(D)** Transferrin uptake is unaffected in HeLa cells over-expressing CLCa or CLCb at either low or high levels, as determined by western blots (top). LC: loading control. **(E)** Transferrin uptake in HeLa cells over-expressing untagged CLCa, or CLCa fused to EGFP at the N- or C-terminus (error bars: s.d. from 3 experiments). **(F)** Transferrin uptake in stably transformed BSC1 cells over-expressing either rat or monkey CLCa or genome-edited to express monkey CLCa-RFP from its endogenous locus, as indicated (error bars: s.d. from 3 experiments).

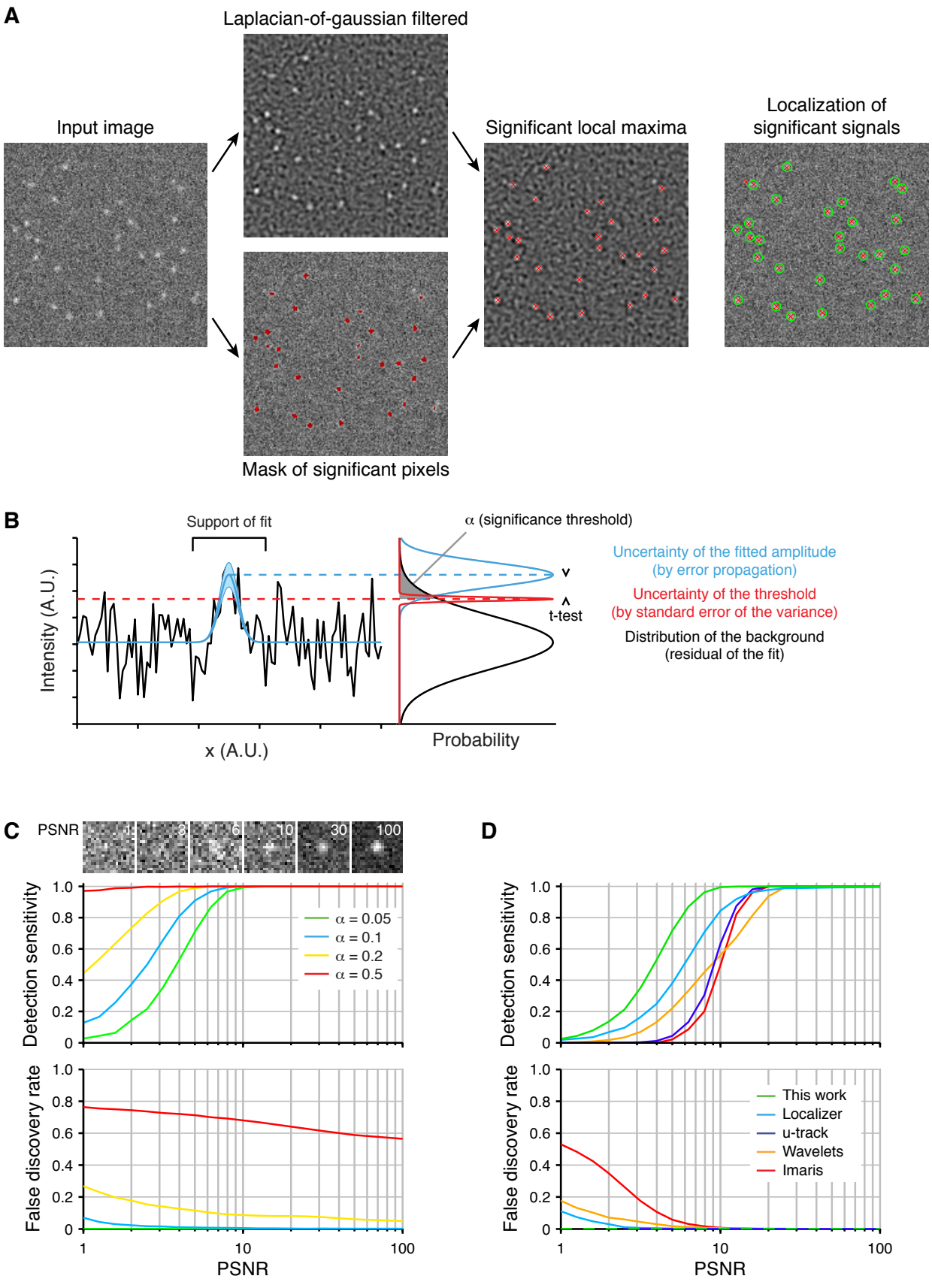

Figure S2. Model-based detection of diffraction-limited fluorescence signals, related to Figure 1 (A) Flow of spot detection algorithm on simulated noisy data. Input image is filtered with two separate filters, one based on the detection model to identify pixels with significant signal (see Supplemental Experimental Procedures), and a Laplacian-of-Gaussian

to identify local maxima. Local maxima at significant locations are used to initialize model fitting, which determines estimates of fluorescence signal amplitude, local background, and sub-pixel location (see Supplemental Experimental Procedures). **(B)** Selection of significant spot signals, illustrated for a 1-D cross-section of a diffraction-limited signal. A Gaussian function approximating the point-spread function (PSF) of the microscope (blue) is fitted to the raw intensities (black), with amplitude, local background, and position as free parameters. The spread of the Gaussian approximation is defined by the PSF. Residuals of the fit yield the noise distribution and, by error propagation, the uncertainty on the fitted amplitude (blue shaded area). The amplitude is considered significant if it lies above a threshold value in the noise distribution, shown here for the 95^{th} percentile. The uncertainty on this threshold is calculated from the standard error of the variance (red). Significance is determined with a one-tailed, two-sample t-test. For details, see Supplemental Experimental Procedures. **(C)** Performance of the detection as a function of the significance threshold α defined in Panel B, calculated on simulated noisy data containing Gaussian-shaped signals of varying amplitude with additive white Gaussian noise, corresponding to a PSNR ranging from 1 to 100 (PSNR was defined as $\max(\text{signal})^2/\text{MSE}$ and MSE is the mean squared error between the true and noisy signal). Detection sensitivity is the proportion of correctly identified signals, and the false discovery rate is the ratio of false positive detections to total detections. **(D)** Comparison of detection performance between the proposed algorithm and several state-of-the-art methods. Performance was assessed on simulated noisy data containing Gaussian-shaped signals of varying amplitude with additive white Gaussian noise, corresponding to a PSNR ranging from 1 to 100. All algorithms were tested using their default, automatic settings unless otherwise noted. The standard deviation of the Gaussian spots was set to 1.4 pixels. Wavelets denotes an approach using wavelet multi-scale products previously used for CCP and endosome detection (Loerke et al. 2009, Olivo-Marin 2002); Imaris denotes the DetectSpots2 function included in the Imaris 7.5 software package, where a spot diameter of 5 pixels was selected. This method was used by (Doyon et al., 2011) for CCP detection based on endogenously labeled CLCa and dynamin; u-track denotes the u-track software package (Jaqaman et al., 2008); Localizer denotes the Localizer software package designed for STORM/PALM applications. The method relies on a generalized likelihood ratio test to assess significance (Dedecker et al., 2012), with 'glrt' parameter set to 15 (at the default value of 25, its performance is slightly inferior to u-track).

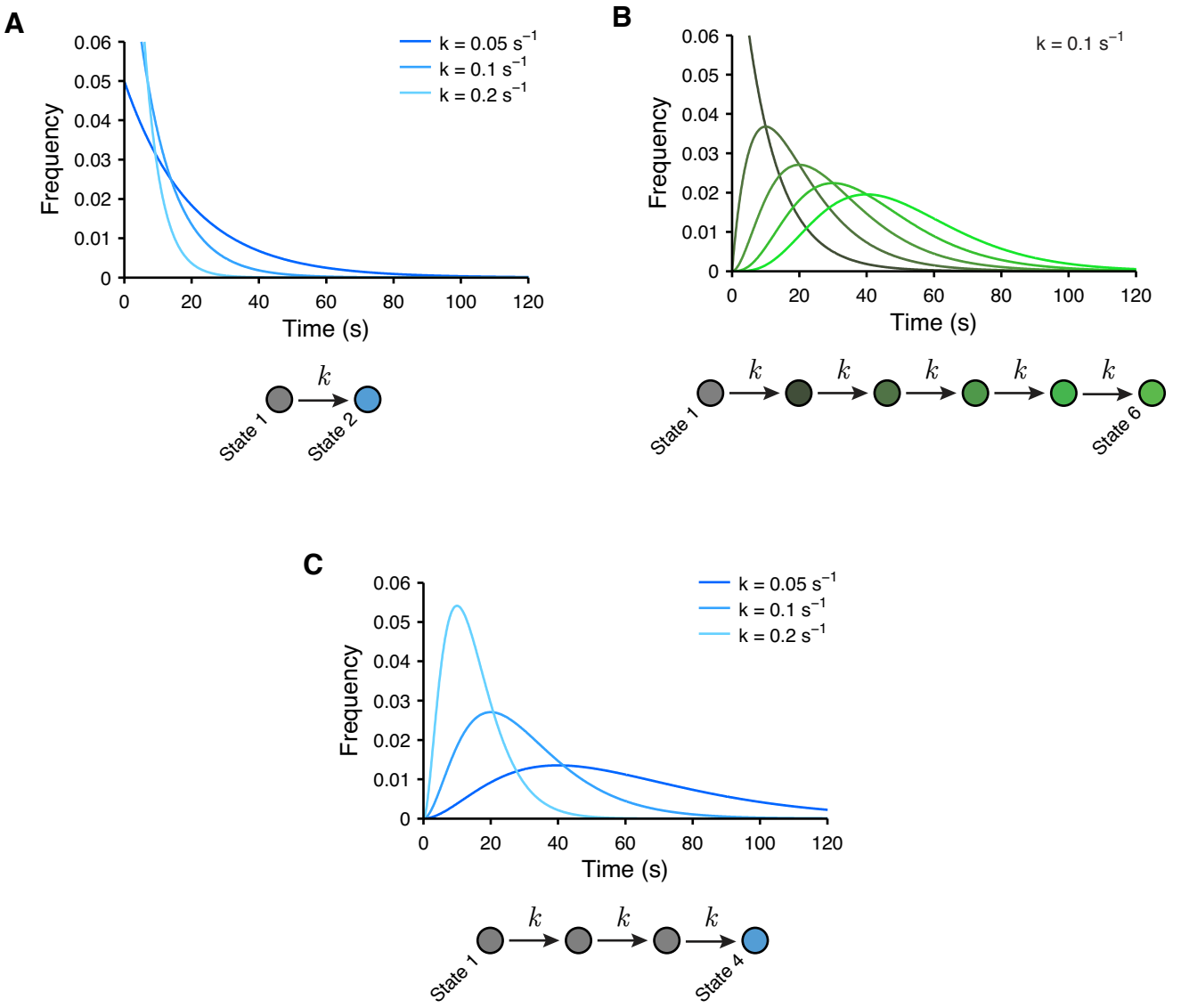

Figure S3. Lifetime distributions generated by single-step and regulated multi-step processes, related to Figure 3 (A) An unregulated process driven by a single rate constant *k* generates exponentially distributed lifetimes. **(B)** A process regulated by transitions through multiple states yields lifetime distributions that display a characteristic rise and decay. The distributions become more spread and are shifted towards longer lifetimes as the number of steps increases. Processes with variable rates among the different steps generate distributions with shapes comparable to those shown. **(C)** For a fixed number of steps, changes in the rate constant(s) produces a scaling effect. Limited to the models described here, the lifetime distribution of CCPs that recruited dynamin (Figure 5, Panel E) is best reproduced by a three-stage process. This is consistent with the statistical decomposition of lifetime distributions in (Loerke et al., 2009), which revealed three populations of CCPs.

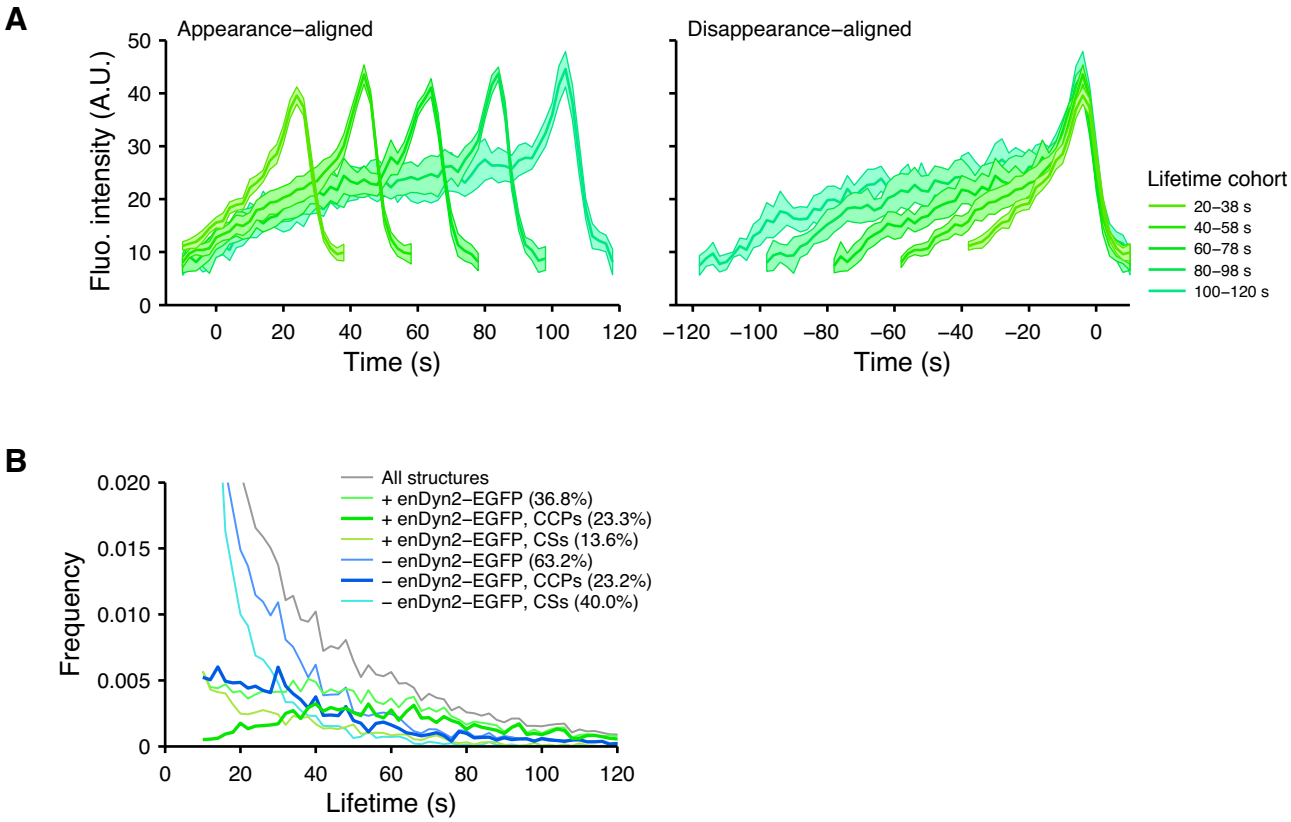

Figure S4. Measurement of dynamin recruitment, related to Figure 5 (A) Average traces of dynamin fluorescence intensity in SK-MEL-2 cells with endogenously-tagged enDyn2-EGFP and overexpressing tdTomato-CLCa. Trajectories were selected for CCPs that recruited detectable enDyn2-EGFP. Averages were calculated for each indicated lifetime cohort from trajectories interpolated to the mean cohort lifetime, and were subsequently aligned by their first (left) or last time point (right). **(B)** Lifetime distributions of all CCSs classified as a function of enDyn2-EGFP recruitment and the intensity threshold described in Figures 2 & 3.

Supplemental Movies

Movie S1. Model-based detection of clathrin-coated structures in EGFP-CLCa over-expressing cells imaged by TIRFM, related to Figure 1. The movie corresponds to the EGFP-CLCa O/X frames shown in Figure 1, Panel A. Red patches indicate pixels detected as significant by a wavelet-based method and green circles indicate the positions of CCSs detected with the model-based algorithm proposed in this work (see Supplemental Experimental Procedures). False-positives (orange circles) and false-negatives (white circles) of the wavelet-based method are in reference to the model-based detections. Scale bar: 2 μm.

Movie S2. Model-based detection of clathrin-coated structures in genome-edited enCLCa-RFP cells imaged by TIRFM, related to Figure 1. The movie corresponds to the enCLCa-RFP frames shown in Figure 1, Panel A. Red patches indicate pixels detected as significant by a wavelet-based method and green circles indicate the positions of CCSs detected with the model-based algorithm proposed in this work (see Supplemental Experimental Procedures). False-positives (orange circles) and false-negatives (white circles) of the wavelet-based method are in reference to the model-based detections. Scale bar: 2 μm.

Movie S3. Master/slave detection of CCSs by μ2-EGFP in genome-edited enCLC-RFP cells, related to Figure 4. CCSs were detected in the μ2-EGFP "master" channel (green circles); fluorescence intensities in the enCLCa-RFP "slave" channel were measured by sub-pixel localization at the detected μ2-EGFP positions (red circles). The small shifts between the positions in the master and slave channels (overlay) are due to the effect of noise on the individual localizations and the motion of CCSs between acquisitions of the two channels. Scale bar: 2 μm.

Movie S4. Master/slave detection of early dynamin recruitment in genome-edited enDyn2-EGFP cells overexpressing tdTomato-CLCa, related to Figure 5. CCSs were detected in the tdTomato-CLCa "master" channel (red circles); fluorescence intensities in the enDyn2-EGFP "slave" channel were measured by sub-pixel localization at the detected tdTomato-CLCa positions. Color code: green, independently detectable enDyn2-EGFP; blue, significant enDyn2-EGFP fluorescence relative to enDyn2-EGFP fluorescence outside of CCSs; gray, undetectable enDyn2-EGFP. The small shifts between the positions in the master and slave channels (overlay) are due to the effect of noise on the individual localizations and the motion of CCSs between acquisitions of the two channels. Scale bar: 2 μm**.**

SUPPLEMENTAL EXPERIMENTAL PROCEDURES

Cells and cell culture

RPE (retinal pigment epithelial) cells stably expressing EGFP-CLCa were generated through infection with retroviruses (described in (Liu et al., 2008)) coding for EGFP-CLCa in a pMIEG3 vector, followed by FACS sorting. SK-MEL-2 (Human Skin Melanoma) cells, expressing CLCa-RFP and/or Dyn2-EGFP under the endogenous promoter were kindly provided by D. Drubin (University of California, Berkeley). As indicated, these cells were transiently transfected with dtTomato-CLCa (kindly provided by T. Kirchhausen, Harvard Medical School) or the μ2 subunit of AP2, tagged with EGFP that was inserted between residues 236 and 237 of an internal disordered loop (kindly provided by S. Sorkin, University of Pittsburgh Medical School), using Lipofectamine 2000 (Life Technologies, Carlsbad, CA) according to the manufacturer's instructions. RPE cells stably expressing full-length (FL) or ΔAD α-adaptin were generated as follows: cDNA encoding the FL or truncated ΔAD α-adaptin, kindly provided by M.S. Robinson (Motley et al., 2006), were subcloned into the pMIEG3 retroviral vector. cDNA encoding mTagBFP (Subach et al., 2008) was subcloned into an IRES downstream of the α-adaptin sequence within the pMIEG3 vector. Each α-adaptin pMIEG3-mTagBFP construct was used to generate retroviruses. RPE cells stably expressing EGFP-CLCa were infected with each resulting retrovirus, followed by FACS to sort cells into nearly homogenous BFP expression cohorts. Note that BFP expression is proportional to the expression of each α-adaptin protein. Expression of α-adaptins within each stable cell cohort was determined by Western blotting with α-adaptin antibodies; the cohort with the expression level closest to endogenous α-adaptin was chosen for further experiments. Cells infected with similar retroviruses expressing only BFP served as the BFP control. All cells were grown under 5% CO2 at 37°C in DMEM/Ham's F12 medium supplemented with 20 mM HEPES, 10 mg/ml streptomycin, 66 µg/ml penicillin and 10% (v/v) and fetal calf serum (FCS, HyClone).

siRNA transfection

RPE cells were treated with a previously established siRNA sequence (Motley et al., 2006) using RNAiMAX (Life Technologies, Carlsbad, CA) to silence endogenous α-adaptin following the manufacturer's instructions. Briefly, 110 pmol of α-adaptin siRNA and 6.25 μl of RNAiMAX reagent were added in 2 ml of OptiMEM in each well of a 6-well plate of RPE cells for 4 hours. Transfection was performed twice, 72h and 48h prior to experiments. Note that exogenous FL or ΔAD α-adaptin (Motley et al., 2006) harbor mutations that confer resistance to siRNA silencing.

Transferrin receptor internalization

Transferrin (Tfn) internalization was performed as previously described (Yarar et al., 2005), using either biotinylated Tfn (BSST) or biotinylated anti-TfnR mAb, B-D65, as ligand. Briefly, RPE cells grown on 15-cm dishes were detached with PBS supplemented with 5 mM EDTA and resuspended in Tfn assay buffer (PBS supplemented with 1 mM $MgCl_2$, 1 mM $CaCl_2$, 5 mM glucose, and 0.2% bovine serum albumin). Suspended cells were incubated with either 5 μg/ml BSST or B-D65 at 37ºC for indicated times followed by immediate cooling to 4ºC to arrest internalization. Following washing to remove unbound ligand, surface bound ligand was quenched by sequential incubation with free avidin (0.05 mg/ml) and biocytin (0.05 mg/ml). Cell lysates were prepared by solubilization in blocking buffer (1% TX-100, 0.1% SDS, 0.2% BSA, 50 mM NaCl, and 1 mM Tris, pH 7.4) and plated onto ELISA plates coated with anti-transferrin (Scottish Antibody Production Unit, Carluke, Scotland) or anti-msIgG (Sigma-Aldrich) and assayed for protected/internalized B-ligand using streptavidin-POD (Roche). Internalized ligand is expressed as the percent of the total surface bound at 4°C (i.e., not quenched with avidin), measured in parallel.

Clathrin heavy chain immunoprecipitation

RPE cell lines either stably expressing CLCa/b fusion proteins or infected with adenoviruses encoding EGFP-CLCa/b or CLCa/b-EGFP were lysed in 250-400 μl buffer containing 50 mM HEPES, pH 7.4, 300 mM NaCl, 5 mM EDTA and 1% TX-100 and protease inhibitor cocktail (Sigma-Aldrich). Cell lysates were passed through a 27.5 gauge syringe 5 times and cell debris was removed by centrifugation at 12k rpm for 15 min. X22 anti-clathrin antibodies were pre-bound to Protein G Sepharose 4 (GE Healthcare) and then incubated with the cell lysates for 4h under constant rotation. Subsequently, unbound proteins were removed and beads were washed 5 times by sequential centrifugation and resuspension in wash buffer (50 mM HEPES, pH 7.4, 300 mM NaCl, 5 mM EDTA and 0.1% TX-100). Immuno-precipitated proteins were

resolved by SDS-PAGE followed by immunoblotting with either anti-clathrin heavy chain (TD.1) or an anti-CLC rabbit polyclonal generated in the Schmid lab.

Immunoblotting

Whole cell lysates were prepared from cells grown on six-well plates as previously described (Antonescu et al., 2010). Briefly, cells were lysed by adding 300 µl of 2× Laemmli sample buffer (2× LSB: 0.125 M Tris, pH 6.8, 2% SDS (wt/vol), 5% glycerol (vol/vol), and 7.5% β-mercaptoethanol (vol/vol), supplemented with protease inhibitor cocktail (Sigma-Aldrich). Equal amounts of total protein of each sample were resolved by SDS-PAGE followed by immunoblotting using the following antibodies: anti-endogenous α-adaptin (100/2, Sigma-Aldrich), anti-exogenous α-adaptin (Motley et al., 2006), anti-β1/2 adaptin (100/1, Sigma-Aldrich), µ2-adaptin (AP-50, BD Transduction Labs). Anti-HSP40 (Enzo Life Sciences) was used as a loading control.

TIRF microscopy

Total internal reflection fluorescence (TIRF) microscopy was performed as previously described (Loerke et al., 2009). Briefly, RPE cells expressing EGFP-CLCa were imaged using a 100× 1.49 NA Apo TIRF objective (Nikon) mounted on a Ti-Eclipse inverted microscope with equipped with the Perfect Focus System (Nikon). During imaging, cells were maintained in DMEM lacking phenol red and supplemented with 2.5% fetal calf serum. Time-lapse image sequences from different cells were acquired at a frame rate of 1 frame·s^{-1} and exposure time of 100-120ms using a CoolSNAP HQ2 monochrome CCD camera with 6.45×6.45 μm^2 pixels (Photometrics, Tuscon, AZ). Similarly, nearly simultaneous 2-channel (e.g. 488 nm epifluorescence/TIRF or 488nm/561nm TIRF) movies were acquired at 0.5 frame·s^{-1} with exposure times for epifluorescence excitation of 50-100 ms (overexpressed EGFP-CLCa), and for TIRF excitation of 100-200 ms (overexpressed EGFP-CLCa or tdTomato-CLCa) or of 900 ms (CLCa-RFP and Dyn2-EGFP under the endogenous promoter).

Image and data analysis

All image and data analyses were carried out in Matlab (MathWorks, Natick, MA), using custom-written software. The software is available for download as Supplementary Software. This version constitutes a snapshot of the software at the time of publication and will not be maintained. Up-to-date versions of the software will be made available at http://lccb.hms.harvard.edu/software.html.

Automated detection of clathrin-coated structures

Diffraction-limited fluorescence signals are most accurately measured by fitting with a model of the microscope point spread function (PSF), which is equivalent to deconvolution of the position and intensity of the fluorescent source. This approach has been widely applied to single molecule tracking (Jaqaman et al., 2008; Sergé et al., 2008) and super-resolution microscopy based on localization of fluorescent emitters such as PALM and STORM (Patterson et al., 2010). In practice, the PSF for in-focus signals is well approximated by a 2-D Gaussian function, which renders the numerical fitting of millions of individual signals computationally tractable.

Algorithms for Gaussian-based detection and localization of fluorescent point sources generally comprise three sequential operations: 1) identification of locations with sufficient probability of containing a point-source signal; 2) estimation of the intensity and sub-pixel localization of these signals by numerical fitting with a 2-D Gaussian; 3) selection of signals considered statistically significant. Step 1) typically consists in selecting the local maxima of a denoised or smoothed version of the input image. The robustness of the criteria applied during Step 3) directly influences the sensitivity and selectivity of the approach. In super-resolution applications where SNR is generally high due to the absence of a strong background signal, a hard threshold on the amplitudes of the fitted signals relative to the estimated variance of the background noise is generally applied (Henriques et al., 2010; Holden et al., 2011; Wolter et al., 2012). As an alternative to such thresholds, which become arbitrary at lower SNRs, an approach testing for the presence of a significant signal by means of a generalized likelihood ratio test has been proposed and shown to improve detection performance (Dedecker et al., 2012).

In this work, we show that by taking into account the uncertainties of the fitted amplitude and local background when individually testing for the significance of each candidate signal, detection sensitivity and selectivity can be significantly increased over existing single-molecule detection methods. This constitutes the key innovation of the proposed detection approach.

In the derivation of this framework, we make the assumption that the fluorescent signals measured from CCSs can be described by a Gaussian PSF function and by an additive white Gaussian noise term. For the signal and noise levels observed on our experimental setup this is a valid approximation, confirmed by testing for normality with the Anderson-Darling test on areas of homogenous background and the residuals of individual fits (note that for photon counts greater than ~20, the Poisson distribution is statistically indistinguishable from a Gaussian, up to a shift in mean). We also assume that the background fluorescence signal beneath each CCS can be locally approximated as constant.

To maximize computational efficiency, the proposed approach was implemented in two steps: a first pass where the amplitude and background are estimated at each pixel by fitting a Gaussian centered on the pixel; this is achieved via linear combinations of three filtering steps and yields a mask of candidate locations for fitting. In the second step, local maxima of the smoothened input image that coincide with this mask are used for initialization of a 2D-Gaussian PSF fit that yields sub-pixel localization and precise estimation of the fluorescence intensity emitted by each CCS.

The image of a CCS was modeled as

$$h[\boldsymbol{x};\boldsymbol{\mu},A,c] = Ag[\boldsymbol{x};\boldsymbol{\mu},\sigma] + c + n[\boldsymbol{x}]$$

where $\boldsymbol{x} = [x_1, x_2]$ are discrete pixel coordinates, A is the fluorescence amplitude, c is a constant representing the local background intensity for this CCS, and $g[\boldsymbol{x};\boldsymbol{\mu},\sigma] = \exp(-((x_1-\mu_1)^2 + (x_2-\mu_2)^2)/(2\sigma^2))$ defines the Gaussian approximation of the microscope PSF. The standard deviation σ is a fixed parameter and will be omitted from the notation for simplicity. The estimation of σ is described at the end of this section. Noise was assumed to follow a Gaussian distribution with standard deviation σ_r over the support of the CCS, i.e., $n[\boldsymbol{x}] \sim \mathcal{N}(0, \sigma_r^2)$. The parameters $\boldsymbol{\mu}$, A and c of the model were estimated around a candidate location $\boldsymbol{k} = [k_1, k_2]$ in an image frame $f[\boldsymbol{x}]$ by sub-pixel localization through the minimization of

$$v = \sum_{\boldsymbol{x}\in S} (h[\boldsymbol{x};\boldsymbol{\mu},A,c] - f[\boldsymbol{k}-\boldsymbol{x}])^2 \qquad (1)$$

The spatial support for this minimization was defined as $S: \boldsymbol{x} \in (-\lceil 4\sigma \rceil, \dots, \lceil 4\sigma \rceil) \times (-\lceil 4\sigma \rceil, \dots, \lceil 4\sigma \rceil)$ centered on $\boldsymbol{k}$. CCS fluorescence was considered significant and retained for further analysis if the estimated amplitude $\hat{A}$ was above a defined threshold level of the local background noise distribution (see below).

Step 1) Pixel-level identification of statistically significant signals

Candidate positions for Gaussian-shaped signals may be obtained as the local maxima of a Laplacian-of-Gaussian-filtered (LoG) version of the input image. In noisy data containing sparse signals such as CCS fluorescence, most of the positions returned by this approach correspond to small fluctuations in the background rather than true signal positions. Performing a Gaussian fit at each position to determine signal strength is computationally inefficient and becomes intractable when applied to the $>10^7$ of positions detected in the frames of a typical time-series. This can be circumvented by first calculating estimates of A and c at the pixel locations of f to generate a pixel-level mask of significant signal positions. Sub-pixel localization can then be performed for the LoG local maxima that fall within this mask (see Figure S2). A pixel-level mask of significant signal positions is obtained by minimizing

$$v = \sum_{\boldsymbol{x}\in S} (h[\boldsymbol{x};\boldsymbol{0},A,c] - f[\boldsymbol{k}-\boldsymbol{x}])^2$$

at each pixel $\boldsymbol{k}$ in frame f, i.e., by minimizing

$$v[\boldsymbol{k}] = \sum_{\boldsymbol{x}\in S} (Ag[\boldsymbol{x}] + c - f[\boldsymbol{k}-\boldsymbol{x}])^2$$

where $g[\boldsymbol{x}]$ denotes $g[\boldsymbol{x};\boldsymbol{0}]$. Specifically, estimates of the amplitude A and local background c for the Gaussian centered at each pixel $\boldsymbol{k}$ are obtained by solving the system

$$\frac{\partial v[\boldsymbol{k}]}{\partial A} = \sum_{\boldsymbol{x}\in S} 2g[\boldsymbol{x}](Ag[\boldsymbol{x}] + c - f[\boldsymbol{k}-\boldsymbol{x}]) = 0$$

$$\frac{\partial v[\boldsymbol{k}]}{\partial c} = \sum_{\boldsymbol{x}\in S} 2(Ag[\boldsymbol{x}] + c - f[\boldsymbol{k}-\boldsymbol{x}]) = 0$$

which yields

$$\hat{A}[\boldsymbol{k}] = \frac{\sum_{\boldsymbol{x}\in S} f[\boldsymbol{k}-\boldsymbol{x}]\, g[\boldsymbol{x}] - \frac{1}{n}(\sum_{\boldsymbol{x}\in S} g[\boldsymbol{x}])(\sum_{\boldsymbol{x}\in S} f[\boldsymbol{k}-\boldsymbol{x}])}{\sum_{\boldsymbol{x}\in S} g[\boldsymbol{x}]^2 - \frac{1}{n}(\sum_{\boldsymbol{x}\in S} g[\boldsymbol{x}])^2}$$

$$\hat{c}[\boldsymbol{k}] = \frac{\sum_{\boldsymbol{x}\in S} f[\boldsymbol{k}-\boldsymbol{x}] - \hat{A}[\boldsymbol{k}] \sum_{\boldsymbol{x}\in S} g[\boldsymbol{x}]}{n}$$

where n is the number of pixels in S. By defining $\gamma_1 = \sum_{\boldsymbol{x}\in S} g[\boldsymbol{x}]$ and $\gamma_2 = \sum_{\boldsymbol{x}\in S} g[\boldsymbol{x}]^2$ (this is numerically more accurate than using the corresponding analytical values), the above equations can be rewritten as

$$\hat{A}[\boldsymbol{k}] = \frac{(f * g)[\boldsymbol{k}] - \frac{1}{n}\,\gamma_1 (f * u)[\boldsymbol{k}]}{\gamma_2 - \frac{1}{n}\,{\gamma_1}^2}$$

$$\hat{c}[\boldsymbol{k}] = \frac{(f * u)[\boldsymbol{k}] - \,\gamma_1 \hat{A}[\boldsymbol{k}]}{n}$$

where $*$ denotes convolution and $u[\boldsymbol{x}]$ is a summation filter defined over S, i.e., $u[\boldsymbol{x}] = 1 \text{ if } \boldsymbol{x} \in S;\ 0 \text{ otherwise.}$

To identify pixels with a significant value of $\hat{A}$ by means of a statistical test, estimates of the uncertainties on $\hat{A}$ and the background noise, given by the residuals of the fit, are needed. At each pixel $\boldsymbol{k}$, the residual sum of squares (RSS) of the fit is given by

$$\mathrm{RSS}[\boldsymbol{k}] = \gamma_2 \hat{A}[\boldsymbol{k}]^2 - 2\hat{A}[\boldsymbol{k}]\big((f * g)[\boldsymbol{k}] - \gamma_1 \hat{c}[\boldsymbol{k}]\big) + (f^2 * u)[\boldsymbol{k}] - 2\hat{c}[\boldsymbol{k}](f * u)[\boldsymbol{k}] + n\hat{c}[\boldsymbol{k}]^2$$

and the variance of the residuals is calculated as

$$\sigma_r^2[\boldsymbol{k}] = \frac{\mathrm{RSS}[\boldsymbol{k}] - (\gamma_1 \hat{A}[\boldsymbol{k}] + n\hat{c}[\boldsymbol{k}] - (f * u)[\boldsymbol{k}])/n}{n-1}$$

The uncertainty (standard deviation) on $\hat{A}[\boldsymbol{k}]$ is obtained by error propagation:

$$\sigma_A[\boldsymbol{k}] = \sqrt{\frac{\mathrm{RSS}[\boldsymbol{k}]}{n-3}[(\mathbf{J}^{\mathbf{T}}\mathbf{J})^{-1}]_{1,1}}$$

where $\mathbf{J} = [\mathbf{g}\ \mathbf{1}]$ is the Jacobian matrix (identical for all pixel positions), and $\mathbf{g}$ is the column-vector representation of $g[\boldsymbol{x}]$ and $\mathbf{1}$ is the unit vector. The probability densities of the fluorescence amplitude and noise in support S at each pixel are thus $\mathcal{N}(\hat{A}[\boldsymbol{k}], \sigma_A^2[\boldsymbol{k}])$ and $\mathcal{N}(0, \sigma_r^2[\boldsymbol{k}])$, respectively.

An estimated amplitude was considered significant if its value was above a threshold value $\kappa\sigma_r$ of the noise distribution, where $\kappa = \sqrt{2}\mathrm{erf}^{-1}(1-2\alpha)$ and α is the significance level (i.e., $\alpha = 0.05$). Significance was determined using a one-sided, two-sample t-test with $H_0: \hat{A} \leq \kappa\sigma_r$, yielding the statistic

$$T[\boldsymbol{k}] = \sqrt{n}\ \frac{\hat{A}[\boldsymbol{k}] - \,\kappa\,\sigma_r[\boldsymbol{k}]}{\sqrt{\sigma_A^2[\boldsymbol{k}] + \kappa^2 s_r^2[\boldsymbol{k}]}} \qquad (2)$$

where the uncertainty on σ_r was calculated using an estimator for the standard error of the variance:

$$s_r[\boldsymbol{k}] \approx \frac{\sigma_r[\boldsymbol{k}]}{\sqrt{2(n-1)}}$$

A mask of significant pixels was then defined as $m[\boldsymbol{k}] \coloneqq\ p[\boldsymbol{k}] < \alpha$, where p is the p-value of the test.

Step 2) Sub-pixel localization and amplitude estimation

Candidate locations for 2-D Gaussian fitting were identified by selecting the local maxima of the Laplacian-of-Gaussian filtered input image that coincided with the mask $m[\boldsymbol{k}]$ (see Figure S2). The standard deviation of the underlying Gaussian kernel was σ.

At each candidate location, a Gaussian fit was performed by minimization of Eq. 1, yielding estimates of A, c and $\boldsymbol{\mu}$ at sub-pixel resolution. The significance of the resulting amplitude estimate $\hat{A}$ was then tested using Eq. 2.

In areas of high CCS density, individual local maxima occurring within the same mask region were either localized individually, or through a mixture-model extension of the proposed approach replacing the single Gaussian in Eq. 1 with a sum of Gaussians. In the latter case, automated selection of the optimal number of mixture components was performed based on iterative F-tests incrementally identifying the statistical justification for additional components. In all instances, each estimated amplitude was individually tested for significance based on the criterion of Eq. 2.

The algorithm was implemented as a C/MEX function for Matlab (MathWorks, Natick, MA) using non-linear optimization routines from the GNU Scientific Library (http://www.gnu.org/software/gsl/). These routines provide a robust and efficient implementation of the widely used Levenberg-Marquardt algorithm.

The standard deviation σ of the 2-D Gaussian PSF was calculated either by fitting a Gaussian to a physical PSF model (Aguet et al., 2009), or by running the fitting step of the algorithm on a limited set of frames with σ as a free parameter, and selecting the most probable value. On the imaging setup used, the two approaches yielded values in agreement within <10% of each other.

Automated tracking of clathrin-coated structures

CCS trajectories were calculated from the detections obtained in individual frames using the u-track software package (Jaqaman et al., 2008). Tracking was performed using positional information only (ignoring amplitude values), and merging and splitting of tracks was enabled. CCSs forming in close vicinity (i.e., within the search radius used for linking individual detections) were thus identified as compound tracks. Examples of such tracks include dense and intersecting clusters of CCSs, or larger structures from which multiple CCPs bud off. Compound tracks can contain a combination of splitting events (branching of two trajectories from a parent trajectory) and/or merging events (fusion of two trajectories into a single trajectory).

The principal tracking parameters used were: maximum gap length: 2 or 3 frames; minimum track length: 1 frame; minimum/maximum search radius for CCSs between consecutive frames: 3/6 or 5/10 pixels. The complete set of parameters is given in the table below.

gapCloseParam	
timeWindow	3-4 or larger
mergeSplit	1
minTrackLen	1
diagnostics	0
costMatrices(1)	
funcName	costMatLinearMotionLink2
linearMotion	0
minSearchRadius	3-5
maxSearchRadius	6-10
brownStdMult	3
useLocalDensity	1
nnWindow	timeWindow
kalmanInitParam	[]
diagnostics	[]
costMatrices(2)	
funcName	costMatLinearMotionCloseGaps2
linearMotion	0
minSearchRadius	3-5
maxSearchRadius	6-10
brownStdMult	3*timeWindow
linScaling	[1 0.01]
timeReachConfL	timeWindow
maxAngleVV	[]
gapPenalty	[]
resLimit	[]

For detailed information on these parameters the reader is referred to the Supplementary Materials of (Jaqaman et al., 2008).

Gap closing accuracy

At the SNR levels obtained in EGFP-CLCa O/X cells, the gap-closing mechanism of the u-track software package is capable of identifying and filling in occasional detection misses, which typically last 1 (~60-70% of gaps) or 2 (~20% of gaps) frames. We validated closed gaps by ensuring that intensity levels always exceeded those of true background.

The maximal duration of potential gaps is constrained by the density of CCPs and the existence of hotspots (Nunez et al., 2011). In both cases, individual events occurring in close vicinity may be erroneously linked together. To avoid a high rate of false positive gaps, the duration limit for gaps was therefore set to 3 frames.

Post-processing of tracks

The trajectories returned by the u-track software were further analyzed and processed to identify signals corresponding to complete observations of assembling CCSs, as opposed to partial tracks, or compound tracks arising from ambiguities in tracking overlapping detections in areas with a high density of CCSs. This was achieved through the following steps:

1. Conversion of simple compound tracks

Compound tracks that consisted of a primary track from/to which short track segments (<5 frames) split/merged were converted into regular tracks consisting of the primary segment alone. This simplification was conditional on the last time point of each splitting segment occurring before the end of the primary track, and on the first time point of each merging segment occurring after the start of the primary track. The segments discarded in this process corresponded to transient, abortive CCSs assembling in close vicinity to a longer-lived CCS.

2. Calculation of gap values

Gap intensities and positions were calculated by numerically fitting the 2-D Gaussian model used for detection at gap locations. Initializations for the fits were obtained by linear interpolation of the values preceding and following each gap. To avoid random localizations in noise at gaps without a trace signal, the fits were constrained to a radius of 2σ pixels (~200 nm).

3. Calculation of CCS fluorescence preceding and following the detected trajectories

CCS fluorescence prior to the first detected time point and following the last detected time point was estimated for a fixed number of “buffer” frames (typically 5), using sub-pixel localization of the 2-D Gaussian model described above. For each frame of these buffer readouts, the localization was initialized with the values of the signal at the first or last time point of the track, respectively. The localization was considered valid if the resulting position was within 2σ pixels (~200 nm) of the initialization; otherwise, the amplitude and background values were estimated by least squares using the position of the first and last detection, respectively.

4. Categorization and selection of valid CCS trajectories

Tracks were categorized as a function of whether they represented complete, partial (truncated at the beginning or end of the acquisition), or persistent (present throughout the entire acquisition) CCS trajectories, and as a function of gap length relative to the length of the track segments bounding each gap. Only trajectories for which the pre- and post-detection buffers could be fully calculated were considered complete. In order to avoid the inclusion of tracks containing sequences of gaps and frames resulting from the linking of independent short-lived events, tracks were classified based on gap properties in two sequential steps. First, tracks with gaps were considered valid if all gaps either consisted of a single frame, or were bounded by track segments of more than one frame. The maximum intensity distribution of these tracks was then calculated for a range of lifetime cohorts (typically [10-19], [20-39], [40-59], [60-79], [80-124], [125-150] s). In the second step, the remaining tracks with gaps were classified as valid if their maximum intensity was above the 2.5^{th} percentile calculated for the respective lifetime cohort.

Next, tracks were further categorized as a function of the pre- and post-detection buffer intensities. Due to the high densities of CCSs observed in some cells and the limited search radius employed during the tracking step to avoid erroneous linking of independent CCS trajectories, some trajectories were truncated. These trajectories were filtered out based on high buffer intensities. Specifically, tracks were considered valid if the intensities of at least two consecutive frames in each buffer were below the detection threshold, and if the maximum intensity of each buffer was below the maximum intensity of the track.

A further criterion for validity was whether or not the CCSs corresponded to diffraction-limited structures. This was established by testing the residuals of the model fit performed during the detection step. For diffraction-limited objects, where the model is accurate, the residuals were expected to follow a normal distribution. The residuals of each fit were therefore tested for normality using the Anderson-Darling test. Trajectories that contained frames with non-normal residuals were excluded from further analysis.

5. Distinguishing gaps from sequential events

Using the u-track settings as described, CCSs forming in close spatial (~5 pixels) and temporal (≤3 frames) vicinity to the end of a preceding event were linked during the tracking process. Such trajectories were identified based on whether they contained gaps with intensities that were statistically indistinguishable from background. Gaps that occurred as a result of insufficient SNR contained residual intensity that remained statistically distinguishable from background. Furthermore, a spatial criterion was applied to corroborate erroneous linking. The individual positions corresponding to each of the two segments of a candidate trajectory were projected onto the line defined by the centroids of the two segments. If no overlap existed between the 95th and 5th percentiles of the resulting two distributions of positions, the trajectory was split into two independent trajectories.

Multi-channel (master/slave) detection and tracking

For multi-channel data, trajectories were obtained using the detections in the master channel containing the fluorescence of a fiducial marker for CCSs (i.e., clathrin or AP2). Fluorescence intensities in the secondary, or slave, channels were calculated through numerical fitting with the 2-D Gaussian model described for the detection step. The position in the slave channels was a free parameter in the fit in order to compensate both for CCS motion between the acquisitions of the individual channels, as well as for potential shifts due to chromatic aberration. The result of the fit was considered valid if the resulting position was within 3σ pixels (~300 nm) of the position in the master channel, and if the intensity was larger than the intensity estimated by least squares at the master position. Otherwise, the fit was considered failed due to insufficient signal, and least squares estimates of the amplitude and background using the position of the master signal were used instead. At the lowest SNR levels at which CCSs were detected (SNR of ~4-5), the localization accuracy is ~50 nm (determined theoretically using Cramér-Rao lower bounds). The median displacement between detections in the two channels was ~60nm and a shift of ~30 nm due to chromatic aberration and/or misalignment between the two channels was estimated from the CCS localizations; this shift was consistent across all experiments.

Mapping of CCP trajectories independently tracked with *μ*2-EGFP and enCLCa-RFP

The mapping of CCS trajectories independently detected using *μ*2-EGFP and enCLCa-RFP was performed based on spatial proximity and temporal overlap of the signals. Trajectories were paired if the maximal distance between the trajectories was <3 pixels (~300 nm), if there was at least 1 frame of overlap in time, and if the enCLCa-RFP trajectory started at most 5 frames before and ended at most 5 frames after the *μ*2-EGFP trajectory. The last constraint was used to minimize bias from CCSs with insufficient *μ*2-EGFP signal (due to the transient expression) in this analysis.

Calculation of lifetime distributions

Lifetime distributions were calculated from all tracks classified as valid during the post-processing described above. To avoid a potential bias from short tracks generated during the linking/gap closing steps but consisting of independent appearance of CCSs, tracks shorter than 5 frames were excluded from the analysis.

Due to the finite length of time-lapse acquisitions, there is an inherent bias in the lifetime measurement. Independent of the lifetime distribution, the probability of observing a specific lifetime is inversely proportional to that lifetime. Specifically, for a movie of n frames, the longest measurable track is $N = n - b_s - b_e$, where b_s and b_e are the length of the start and end buffer, respectively, in frames. The relative probability of observing a track with lifetime t is $(N - t + 1)/N$. The lifetime distributions were corrected for this factor, as previously described (Loerke et al., 2009).

Threshold for intensity-based decomposition of lifetime distributions

The time interval from the beginning of CCS assembly over which the maximum fluorescence intensity distribution was independent of lifetime was determined by a measure of similarity among these distributions across different lifetime cohorts. Statistical tests for similarity such as Kolmogorov-Smirnov or Anderson-Darling were not a sufficiently robust measure, likely due to heterogeneities in the long upper tails of the distributions. To avoid the influence of these tails, a measure of similarity based on the location of the peaks of the distributions was calculated. This was achieved by least-

squares fitting of a Gaussian function to the first mode of the distribution from each lifetime cohort (cohorts were generally chosen as [1-10], [11-15], [16-20], [21-40], [41-60], [61-120] s). For robustness, values larger than the mean of the Gaussian were excluded from the evaluation of the objective function. The distributions were classified as similar if the means obtained for the different cohorts were within the expected standard error, calculated from the parameters of Gaussian obtained for the first cohort (i.e., [0-10) s). The time interval for the threshold was chosen as the largest interval for which the distributions were similar by this measure. The threshold was chosen as the 95th percentile of the Gaussian fitted to the maximum intensity distribution for that interval, across all CCS trajectories.

Normalization of fluorescence intensities across data sets

To pool intensity values of CCS trajectories from n cells with different expression levels, a scaling factor a_i was determined for each cell i so that the cumulative distribution of maximum CCS intensities $F_i(x)$ in cell i was mapped to a reference distribution $F_{\mathrm{ref}}(x)$ by minimizing $\int (c_i + (1-c_i)F_i(x/a_i) - F_{\mathrm{ref}}(x))^2 \,\mathrm{d}x$. The constant c_i was used to estimate the amount of missing data between each distribution $F_i(x)$ and $F_{\mathrm{ref}}(x)$; that is, between two cells the maximum intensity distribution of the lower-expressing cell is truncated with respect to the distribution of the higher-expressing cell due to a larger percentage of small, low-intensity objects falling below the detection threshold. The reference distribution $F_{\mathrm{ref}}(x)$ was determined by first calculating the median distribution $F_{\mathrm{med}}(x) = \mathrm{median}(F_1(x), \dots, F_n(x))$ between the cumulative maximum intensity distributions of cells 1 to n. Subsequently, the reference distribution $F_{\mathrm{ref}}(x)$ was selected as the distribution among $F_1(x), \dots, F_n(x)$ with the smallest integrated least-squares distance to $F_{\mathrm{med}}(x)$.

Calculation of average intensities as a function of lifetime cohort

Average fluorescence intensities were calculated by interpolating all trajectories within a cohort to a length corresponding to the average lifetime of that cohort. Specifically, the intensities of trajectories in a cohort bounded by lifetimes [t0…t1] s were interpolated to the time vector bounded by [0… (t0+t1)/2)] using cubic B-splines. This enabled the point-by-point averaging of the intensities. The time windows chosen for this averaging (typically in 20s intervals, e.g., [0-20], [20-40], [40-60], [60-80], [80-100], [100-120] s) were sufficiently small to avoid averaging artifacts.

Classification of Dyn2-positive and Dyn2-negative CCPs and calculation of the 'slave' significance threshold

CCP trajectories were classified as positive for a slave signal (e.g. Dyn2-EGFP) if this signal was significant (i.e., detectable independently of tdTomato-CLCa) for longer than a random association. The probability of random detection of a significant slave signal was calculated as follows: 1) A mask of the cell outline was calculated for each time-series by average-projecting all images after exclusion of CCP signals based on the CCP masks calculated as part of the detection process. This projection contained only background signal from inside and outside the cell, and its intensity distribution featured two distinguishable peaks. An intensity threshold was automatically selected as the minimum between these peaks and applied to the projection image to generate a cell mask. 2) The Gaussian PSF model was then fitted at 50000 random locations within the cell in the slave channel, and the significance of each fit was calculated with the t-test described for CCP detection. The fraction of significant fits yielded the probability p of random detection of an independently significant slave signal. For robustness, this probability was averaged across 10 frames evenly selected from each time-series. Trajectories were classified as slave signal-positive if the number of significant slave detections exceeded the number predicted by random association, which for each trajectory is given by the binomial distribution with parameters p and n, where n is the number of time points in the trajectory. Since the time points with significant slave detections in a trajectory were typically clustered, no explicit continuity constraint was enforced in this comparison.

The threshold to determine the significance of slave signals relative to background locations outside of CCPs was calculated using a similar procedure. The Gaussian PSF was fitted at 50000 random locations within the cell, but excluding locations within the CCP mask calculated during the detection step. This yielded a Gaussian-shaped distribution of background fluorescence. The slave significance threshold was selected as the 95th percentile of this distribution. For robustness, this threshold was also calculated across 10 frames evenly selected from each time-series and averaged. Photobleaching had a negligible effect on the value of this threshold and the probability p. To determine the significance of slave signals relative to this threshold at individual detections within a trajectory, a t-test analogous to the test described for detection was applied.

Curvature measurement by Epi:TIR fluorescence ratio

The epifluorescence to TIRF ratio was calculated for each trajectory as the maximum intensity detected in the epifluorescence channel divided by the maximum intensity detected in the TIRF channel. To normalize the intensities

between the two channels such that flat structures at the membrane yielded an Epi:TIR ratio of 1, a multiplicative correction factor was applied. This was calculated as the ratio between the mean intensity of the first detected frame of all trajectories in the TIRF channel relative to the mean intensity of the same set of detections in the epifluorescence channel, assuming that in the first frame of a trajectory CCSs are still flat.

Supplemental References

Aguet, F., Geissbühler, S., Märki, I., Lasser, T., and Unser, M. (2009). Super-resolution orientation estimation and localization of fluorescent dipoles using 3-D steerable filters. Opt. Express *17*, 6829–6848.

Antonescu, C.N., Danuser, G., and Schmid, S.L. (2010). Phosphatidic acid plays a regulatory role in clathrin-mediated endocytosis. Mol. Biol. Cell *21*, 2944–2952.

Dedecker, P., Duwé, S., Neely, R.K., and Zhang, J. (2012). Localizer: fast, accurate, open-source, and modular software package for superresolution microscopy. J. Biomed. Opt. *17*, 126008.

Doyon, J.B., Zeitler, B., Cheng, J., Cheng, A.T., Cherone, J.M., Santiago, Y., Lee, A.H., Vo, T.D., Doyon, Y., Miller, J.C., et al. (2011). Rapid and efficient clathrin-mediated endocytosis revealed in genome-edited mammalian cells. Nat. Cell Biol. *13*, 331–337.

Henriques, R., Lelek, M., Fornasiero, E.F., Valtorta, F., Zimmer, C., and Mhlanga, M.M. (2010). QuickPALM: 3D real-time photoactivation nanoscopy image processing in ImageJ. Nat. Methods *7*, 339–340.

Holden, S.J., Uphoff, S., and Kapanidis, A.N. (2011). DAOSTORM: an algorithm for high- density super-resolution microscopy. Nat. Methods *8*, 279–280.

Jaqaman, K., Loerke, D., Mettlen, M., Kuwata, H., Grinstein, S., Schmid, S.L., and Danuser, G. (2008). Robust single-particle tracking in live-cell time-lapse sequences. Nat. Methods *5*, 695–702.

Liu, Y.-W., Surka, M.C., Schroeter, T., Lukiyanchuk, V., and Schmid, S.L. (2008). Isoform and splice-variant specific functions of dynamin-2 revealed by analysis of conditional knock-out cells. Mol. Biol. Cell *19*, 5347–5359.

Loerke, D., Mettlen, M., Yarar, D., Jaqaman, K., Jaqaman, H., Danuser, G., and Schmid, S.L. (2009). Cargo and dynamin regulate clathrin-coated pit maturation. PLoS Biol. *7*, e57.

Motley, A.M., Berg, N., Taylor, M.J., Sahlender, D.A., Hirst, J., Owen, D.J., and Robinson, M.S. (2006). Functional analysis of AP-2 α and μ2 subunits. Mol. Biol. Cell *17*, 5298–5308.

Nunez, D., Antonescu, C., Mettlen, M., Liu, A., Schmid, S.L., Loerke, D., and Danuser, G. (2011). Hotspots Organize Clathrin-Mediated Endocytosis by Efficient Recruitment and Retention of Nucleating Resources. Traffic *12*, 1868–1878.

Patterson, G., Davidson, M., Manley, S., and Lippincott-Schwartz, J. (2010). Superresolution imaging using single-molecule localization. Annu Rev Phys Chem *61*, 345–367.

Sergé, A., Bertaux, N., Rigneault, H., and Marguet, D. (2008). Dynamic multiple-target tracing to probe spatiotemporal cartography of cell membranes. Nat. Methods *5*, 687–694.

Subach, O.M., Gundorov, I.S., Yoshimura, M., Subach, F.V., Zhang, J., Grüenwald, D., Souslova, E.A., Chudakov, D.M., and Verkhusha, V.V. (2008). Conversion of red fluorescent protein into a bright blue probe. Chem. Biol. *15*, 1116–1124.

Wolter, S., Löschberger, A., Holm, T., Aufmkolk, S., Dabauvalle, M.-C., van de Linde, S., and Sauer, M. (2012). rapidSTORM: accurate, fast open-source software for localization microscopy. Nat. Methods *9*, 1040–1041.

Yarar, D., Waterman-Storer, C.M., and Schmid, S.L. (2005). A dynamic actin cytoskeleton functions at multiple stages of clathrin-mediated endocytosis. Mol. Biol. Cell *16*, 964–975.